# Nanosecond plasma-mediated electrosurgery with elongated electrodes

Alexander Vankov[a] and Daniel Palanker
*Hansen Experimental Physics Laboratory and Department of Ophthalmology, Stanford University, Stanford, California 94305*

(Received 19 May 2006; accepted 10 April 2007; published online 19 June 2007)

Progress in interventional medicine is associated with the development of more delicate and less invasive surgical procedures, which requires more precise and less traumatic, yet affordable, surgical instruments. Previously we reported on the development of the pulsed electron avalanche knife for dissection of soft tissue in liquid media using the 100 ns plasma-mediated electric discharges applied via a 25 $\mu$m disk microelectrode. Cavitation bubbles accompanying explosive vaporization of the liquid medium in front of such a pointed electrode produced a series of craters that did not always merge into a continuous cut. In addition, this approach of surface ablation provided a limited depth of cutting. Application of an elongated electrode capable of cutting with its edge rather than just with its pointed apex faces a problem of nonuniformity of the electric field on a nonspherical electrode. In this article we explore dynamics of the plasma-mediated nanosecond discharges in liquid medium in positive and negative polarities and describe the geometry of an electrode that provides a sufficiently uniform electric field along an extended edge of a surgical probe. A highly enhanced and uniform electric field was obtained on very sharp (2.5 $\mu$m) exposed edges of a planar electrode insulated on its flat sides. Uniform ionization and simultaneous vaporization was obtained along the whole edge of such a blade with 100 ns pulses at 4–6 kV. A continuous cutting rate of 1 mm/s in the retina and in soft membranes was achieved at a pulse repetition rate of 100 Hz. The collateral damage zone at the edges of incision did not exceed 80 $\mu$m. Negative polarity was found advantageous due to the lower rate of electrode erosion and due to better spatial confinement of the plasma-mediated discharge in liquid. © *2007 American Institute of Physics*. [DOI: 10.1063/1.2738374]

## I. INTRODUCTION

Current mechanical approaches toward vitreoretinal surgery carry distinct risks including traction tears and imprecise depth of cutting leading to excessive collateral damage, nicked vessels, etc. Dielectric breakdown-based dissection of tissue with short-pulsed femto-to-nanosecond lasers,[1–3] while helping to reduce traction-related damage and improving cutting precision, is limited in vitreoretinal applications due to the long waist (and thus low axial precision of focusing) of the laser beam in the posterior pole of the eye.[1] In addition, large optical aberrations in the peripheral retina reduce the precision and safety of this procedure, while the light propagating beyond the focal point presents a potential danger to the photosensitive retina.[1,4] Pulsed shallow-penetrating lasers [Er: yttrium-aluminum-garnet (YAG) and ArF excimer] delivered into the eye via optical fibers[5–7] enable localized treatment of tissue with uniform accuracy at all areas. However, these instruments also have failed to achieve widespread acceptance in ocular surgery due to their prohibitively high cost, large size, relatively slow pace, and lack of coagulation regime.[7,8]

To address the disadvantages of both mechanical and laser-based instrumentation for tissue dissection in intraocular surgery, we have designed and previously described a device called pulsed electron avalanche knife (PEAK).[9,10] This instrument uses a high electric field rather than laser photons to create plasma in front of the intraocular probe, and thus it is compact and inexpensive. Recently we have demonstrated[10,11] that PEAK is capable of dissecting the retinal tissue, as well as epiretinal membranes, lens capsule, and lens cortex. However, extensive testing of this device[12] has revealed the following limitations: (1) An inlaid disk microelectrode embedded into an insulating probe cannot penetrate into tissue and thus can only produce shallow cuts on its surface. (2) Cavitation bubbles accompanying each pulse create significant collateral damage in tissue.[12] Reduced pulse energy helps to decrease this mechanical damage, but also leads to decreased cutting depth. (3) A series of perforations in the tissue produced by individual pulses does not always merge into a continuous cut.

In this article we study the dynamics of the submicrosecond electric discharges in liquid media and mechanisms of tissue dissection with such discharges. We also describe a way to overcome some of the limitations listed earlier by using an elongated (penetrating) electrode, which cuts tissue with its edge rather than just with its pointed apex.

## II. MATERIALS AND METHODS

The dynamics of electric discharge in liquid was studied using pointed electrodes similar to the previously described PEAK probes:[10] a tungsten wire of 25 $\mu$m in diameter sealed into a tapered glass capillary and rounded at the end in such a way that only the tip of the wire, i.e., the inlaid disk was exposed to the liquid (see Fig. 1). The glass capillary was

[a]Electronic mail: vankov@stanford.edu

 

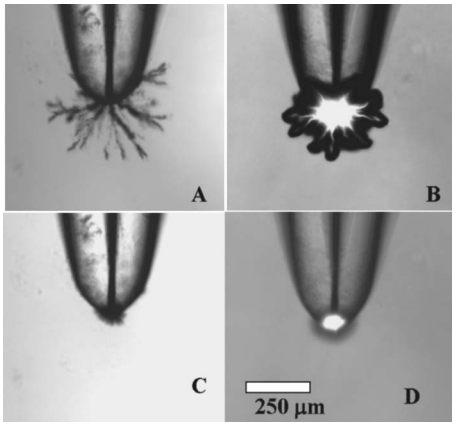


FIG. 1. Photographs of the 6 kV, 500 ns discharges of positive (A, B) and negative (C, D) polarity in de-ionized water (A, C) and in saline (B, D). Photographs have been taken with a single 500 ns flash started with the beginning of the pulse.

tapered from 0.7 mm to about 0.2 mm at the tip for better access to the tissue. This insulated probe was then enclosed in a 20 G (0.92 mm outer diameter) stainless steel needle, which was used as a return electrode. The axial distance between the disk microelectrode and the coaxial needle was about 3 mm.

The homemade pulse generator used in this study was producing pulses of 100–500 ns in duration with an amplitude of up to 10 kV and with a rise and fall time of 50 ns. Total energy of the discharge was limited by a buffer capacitor of 0.1 nF. Experiments with longer pulse durations 500 ns–10 $\mu$s have been performed using pulse generator PVX-4150 (Direct Energy Inc.). Electrode potential was recorded using a Tektronix high voltage probe (1000×, 3 pF), while the current was measured as a voltage drop on a 50 Ω resistor connected between the return electrode and the ground terminal of the pulse generator. The hand piece including a 25 $\mu$m wire sealed inside the glass pipette and the surrounding coaxial needle had a capacitance of about 3 pF. The current charging this capacitor was first measured with an electrode in the air and then subtracted from the current measured during the discharge in a conductive liquid.

Erosion of the metal electrode was measured by imaging the extent of etching of the sealed wire as a function of number of pulses using high magnification microscope with transmission illumination (Nikon TE2000-U, objectives ×20 and ×40).

The dynamics of the cavitation bubbles was studied using fast flash shadow photography on inverted microscope using charge coupled device camera (LN/CCD-512, Princeton Instruments, Inc.). Fast flash was produced by light emitting device (LMR51WF, Sunled Corp.,Walnut Creek, CA) driven by a homemade pulse generator with pulse durations varying from 0.1 to 1 $\mu$s having the rise and fall times of 10 ns. For precise measurements of the boundary velocities we applied rapid sequences of (two or more) flashes recorded on the same frame of the image. Superposition of several photographs with controlled delays allows for accurate measurements of the bubble dynamics even in poorly reproducible events. Light emission by the plasma discharge in liquid was monitored with a fast (20 ns response time) photomultiplier (model R928, Hamamatsu, Japan).

Extent of collateral damage in tissue was assessed using propidium iodide (PI) staining, which is a very sensitive fluorescent indicator of cell membrane permeability.[13,14] PI enters into cells which have lost membrane integrity, whether that loss is transient or permanent, and bind to its preferred target—nucleic acids thus undergoing a 1000 times increase in its fluorescence quantum yield.[13,14]

Electric field in the medium was calculated using FlexPDE-5 software package (PDE Solutions Inc.). Assuming cylindrical symmetry of the problem, the two-dimensional finite element method was applied using 800 nodes.

## III. RESULTS AND DISCUSSION

### A. Streamers

Typical shadow photographs of the 500 ns discharges in de-ionized water and in saline are shown in Fig. 1. These photographs were taken with 500 ns flashes started simultaneously with the beginning of high voltage electric pulses. The width of the streamers (the ionization treks appearing as dark areas in shadow photography in frames A and C) created by positive discharges did not exceed 3 $\mu$m while their length could reach several hundreds of micrometers. The minimal streamer propagation velocity was found by dividing the length of the streamer by the pulse duration. The supersonic velocity of about 3 km/s was detected for positive streamers in both, the de-ionized water and in saline solution. Negative discharges, on the other hand, had very compact hemispherical shape in both, the de-ionized water and in saline. Discharges in a conductive medium generated bright light-emitting plasma (frames B and D) geometrically similar to the dark streamers generated in the de-ionized water (frames A and C).

Several models describing propagation of the streamers in liquids have been developed to date. In thermal models the avalanche is initiated in the bubbles which can be formed due to heating by the ionic prebreakdown currents, or local heating of the liquid by field emission currents.[15–18] "Tree-like" branching behavior of streamers was successfully described by models based on the network of capacitive and resistive elements.[19] In nonthermal models crack propagation occurs by electromechanical stress while ionization occurs in the pre-existing bubbles.[20] Briefly, in a negative discharge (starting on cathode) electrons are ejected from the metal electrode into the filament in liquid and the conductive streamers act as equipotential extensions of the electrode into the liquid.[16,21] The electric field around the equipotential filament is maximal at the apex, where it has almost spherical geometry which promotes formation of a dense bush-like highly branched structure[20] [Figs. 2(a) and 2(c)]. In contrast, in a positive discharge (on anode) electrons are striped from the liquid in the filament and accelerate toward the metal electrode. Due to the relatively low amount of charge carriers in the liquid and low mobility of the remaining positive ions they create uniform surface charge along the boundaries of

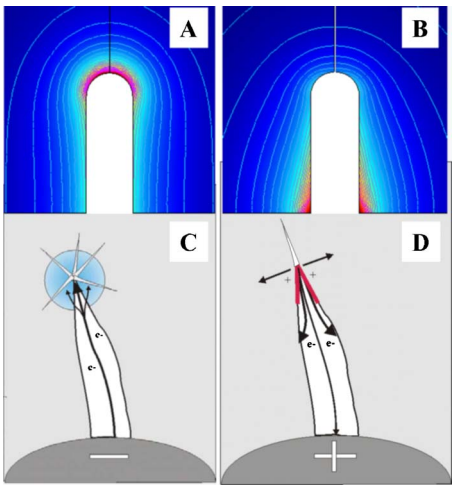


FIG. 2. (Color online) Distribution of the electric field around (a) equipotential filament and (b) a filament with a constant charge density at its surface. Spherical symmetry at the head of the negative streamer induces bifurcations, while the positive filament propagates as a single crack.

the crack[16,21] [Figs. 2(b) and 2(d)]. Either the repulsive forces between the positively charged boundaries of the cylindrical filament (according to the crack model) or vaporization along the boundaries of the cylindrical filament (according to the thermal model) lead to propagation of the crack forward up to hundreds of micrometers, having much less bifurcations than the negative streamers.

### B. Dynamics of the discharge

Typical voltage and current wave forms, as well as light emission by the plasma during positive and negative discharges at 2.1 kV in saline are shown in Fig. 3. Even though, due to depletion of the buffer capacitor, the voltage decreases starting at 100 ns the current continues to rise due to development of the plasma-mediated discharge. Light emission by the plasma starts at 100 ns and increases until the end of the pulse, after which it decays with a characteristic lifetime of about 200 ns.

Conductance of the negative discharge obtained as a ratio of the current to voltage is plotted in Fig. 4. During the first 80 ns the current is very spiky due to the transients induced by the pulse rising edge and due to formation of the plasma streamers in the liquid. Average conductance during the first 80 ns is $71\pm16$ $\mu$Si for all voltage levels. This value is in a good agreement with ionic conductance of saline between the inlaid disk electrode with diameter $d=25$ $\mu$m and a large return electrode at infinity: $\Gamma_0=\gamma 2d=70\mu$Si, where $\gamma=14$ mSi/cm is conductivity of saline.[22] Conductance decreases with time prior to the plasma ignition due to formation of a gas layer disconnecting the electrode from the conductive liquid. Initiation of the plasma occurs earlier at higher voltages—starting with 500 ns at 1 kV and reaching 70 ns at 6 kV. Maximal conductance was higher with positive polarity probably due to the larger size of the streamers (as shown in Fig. 1), making larger contact area with liquid and thus reducing resistance of the liquid.

Latency $t_{pre}$ prior to the moment of ionization decreases with the applied voltage $U$, as shown in Fig. 5(a). This dependence could be closely approximated by the power function $t_{pre}\sim 1/(U-U_{th})$, where $U_{th}$ is the ionization threshold at long pulse durations. $U_{th}$ was measured at pulse durations up to 100 $\mu$s, and was found similar for disk, wire, and blade electrodes, described later. $U_{th}$ was $-200$ V for negative and $+450$ V for positive discharges. Integration of the power (voltage $\times$ current) over time until the moment of ionization allows one to assess the amount of energy $E_{ion}$ deposited prior to plasma ignition. As plotted in Fig. 5(b), $E_{ion}$ increases linearly with the applied voltage. This linear behavior can be explained by the fact that the conductance of the discharge $\sigma$ changes very little prior to ionization (Fig. 4), therefore $E_{ion}$ can be estimated as $E_{ion}=U^2\sigma t_{pre}$. Since in the range of interest $U\gg U_{th}$ $t_{pre}$ can be approximated as $\sim 1/U$, then preionization energy should linearly increase with voltage: $E_{pre}\sim U$. After the moment of ionization conductance of the discharge rapidly increases and the discharge energy increases quadratically with time for pulses of fixed duration, as shown in Fig. 5(b) for 100 and 200 ns durations.

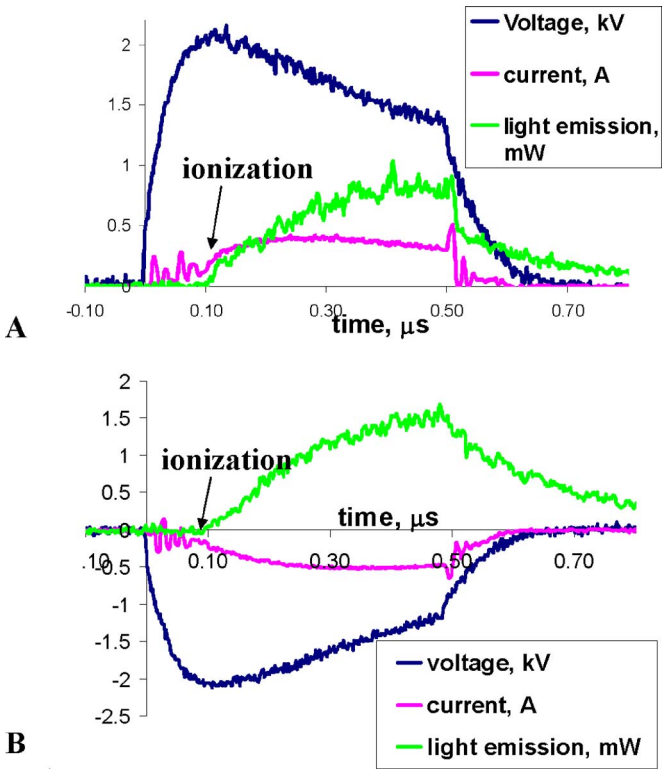


FIG. 3. (Color online) Voltage, current, and light emission for anodic (a) and cathodic (b) discharges.

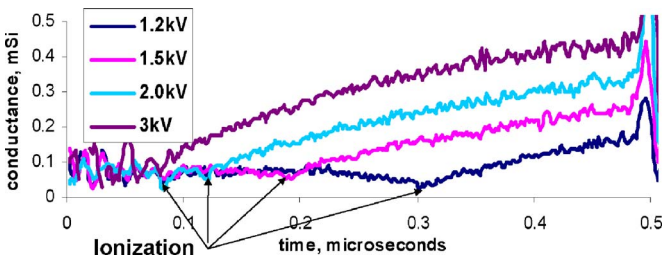


FIG. 4. (Color online) Dynamics of conductance of the negative discharge during 500 ns pulse.

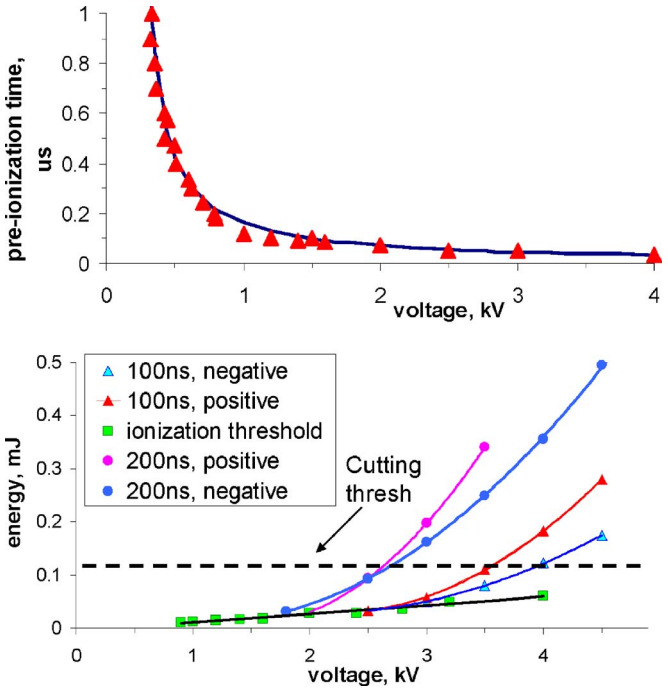


FIG. 5. (Color online) (a) Ionization latency as a function of voltage on inlaid disk electrode. Solid line depicts a fitting function: $t=0.13/(U-0.2)$. (b) Ionization threshold energy for various pulse durations and discharge energy for 100 and 200 ns pulses.

The electric discharge on the inlaid disk microelectrode was accompanied by the growth and collapse of a nearly spherical cavitation bubble. Mechanical energy of a spherical cavity with a volume $V$ can be estimated as $E_{\text{bub}}=P_0V$, assuming that at maximal expansion phase the gas pressure inside it is negligible compared to the ambient pressure $P_0$ in the liquid.[23,24] At pulse durations not exceeding 500 ns 7%±1% of the discharge energy was converted into the mechanical energy of the bubble for both positive and negative polarities. With 100 ns pulses at 4 kV the initial bubble expansion velocity was 32 m/s and its maximal radius was 255 $\mu$m. As shown in Fig. 6, bubble expansion velocity remained practically constant during the first 3 $\mu$s. This observation allows estimating pressure inside the vapor cavity according to the Rayleigh equation[23,24]

$$R\frac{d^2R}{dt^2}+\frac{3}{2}\left[\frac{dR}{dt}\right]^2=\frac{p(R)-p_\infty}{\rho},$$

where $\rho$ is the liquid density, $p_\infty$ is the pressure in the liquid far from the bubble, and $p(R)$ is the pressure in the liquid at the bubble boundary. At constant expansion velocity ($dR/dt=V$, $d^2R/dt^2=0$) the pressure at the bubble boundary can be calculated as

$$p(R)=\frac{3\rho}{2}V^2+p_\infty.$$

For the bubble expansion velocity $V=32$ m/s the pressure is $P=16$ bar, and corresponding temperature of the saturated vapor is 210 °C.[25]

Electric discharges of different polarities were found to erode metal electrodes with very different rates. Negative pulses of 0.15 mJ etched tungsten electrodes with a rate of 0.065 $\mu$m$^3$/pulse, while positive pulses of the same energy had the etching rate higher by more than an order of magnitude: 0.67 $\mu$m$^3$/pulse. For this reason negative polarity is advantageous for surgical applications.

Earlier studies have demonstrated that the primary mechanism of tissue dissection with submicrosecond pulses is mechanical rupturing by rapidly expanding and collapsing cavitation bubbles.[9,11,12] In the current study we observed that the energy of the 100 ns pulse perforating chorioallantoic membrane with 50% probability was $E_{\text{dis}}=49$ $\mu$J (−3 kV, 100 ns), while 100% probability of perforation was achieved at 120 $\mu$J (−4 kV, 100 ns). As shown in Fig. 5, these energy levels exceeded the ionization threshold, or in other words, tissue cutting did not occur without ionization. If not for ionization, a layer of vapor and gaseous products of electrolysis forming at the electrode surface would disconnect it from the electrolyte and stop the current flow, thus precluding delivery of sufficient energy for cutting. Ioniza-

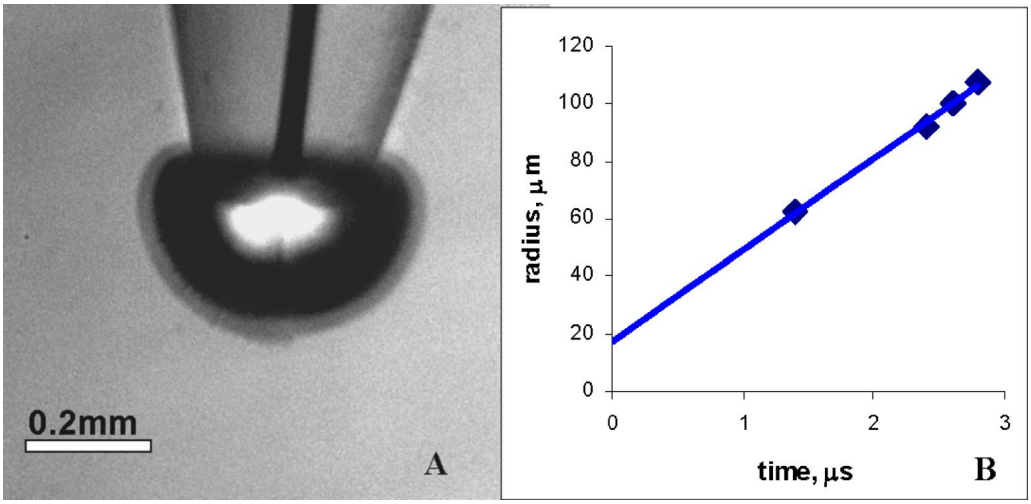


FIG. 6. (Color online) (a) Bubble size and boundary velocity measured with the "double flash" technique after application of a 100 ns pulse at −4 kV. Change in the bubble shape between the two flashes is a gray zone seen at the perimeter. (b) During the first 3 $\mu$s after the discharge bubble expands with a constant boundary velocity of 32 m/s.

tion of the gas solves this problem and allows for delivery of the desirable amount of energy into the medium. Formation of the ionization streamers leads to a rapid increase in conductance, and consequently in the rate of energy deposition. Plasma density in filaments increase, they merge, vapor pressure increases, and rapidly expanding bubble ruptures the adjacent tissue. If the electric pulse continues, the current can further increase and the discharge can develop into an arc between the metal electrode and aqueous medium.[26]

### C. Discharge on elongated electrodes

Pulsed discharges applied via a pointed electrode at the tissue surface produce individual craters, but these craters do not always overlap, so bridges are often left between the two sides of tissue, and thus multiple scans are required to achieve a complete separation of sides. In addition, surface application of an electrode is limited to shallow cutting since, due to the spherical symmetry of the bubble, the depth of the cut is similar to its width.[12] A more useful tool would be the one that (a) allows for deep cutting and (b) completely separates two sides during one scan.

Long electrode cutting tissue with its side rather than just with its apex would address this issue. However, elongated electrode typically has a very nonuniform electric field [Fig. 7(a)], so vaporization and ionization would occur primarily at its apex, where the field is highest, as exemplified in Fig. 7(b).

This problem could be solved by folding a wire electrode into a loop, thus eliminating such singular points. However, to achieve high electric fields and low threshold energies the long wire should be very thin (below 25 $\mu$m), which makes such tool very flimsy and poorly visible in a surgical microscope.

We addressed this problem by designing an electrode as a blade insulated on both planar surfaces and exposed to a conductive medium at the sharp edges [Fig. 7(a)]. The exposed edge is electrically equivalent to a loop electrode made of a very thin wire, but it is very sturdy and easily visible due to large width of the blade. With a radius of curvature at the edge being 2.5 $\mu$m, the electric field at the electrode surface reaches 2 MV/cm with a 3 kV electric pulse. Streamer formation at the edge of the blade was observed in de-ionized water at 3 kV with a pulse duration of 100 ns. In saline a thin layer of plasma was forming along the whole length of the exposed edge, accompanied by a ring of cavitation bubbles uniformly covering the blade, as shown in Fig. 8. Even if the blade is not round, the electric field along its edge is rather uniform as long as there are no singular points, i.e., as long as the planar radius of curvature of the blade is much larger than the thickness of its sharp edge.

The ionization threshold voltage on a 25 $\mu$m inlaid disk was very similar to that of a blade electrode of 200 $\mu$m in length and 5 $\mu$m in width, as shown in Fig. 9(a). It decreased from about 2 kV at 100 ns down to a constant level of 0.42 kV at pulse durations exceeding 3 $\mu$s. The corresponding ionization threshold energy on a disk electrode decreased with pulse duration, as shown in Fig. 9(b). This trend is consistent with the plots shown in Fig. 5, where ionization

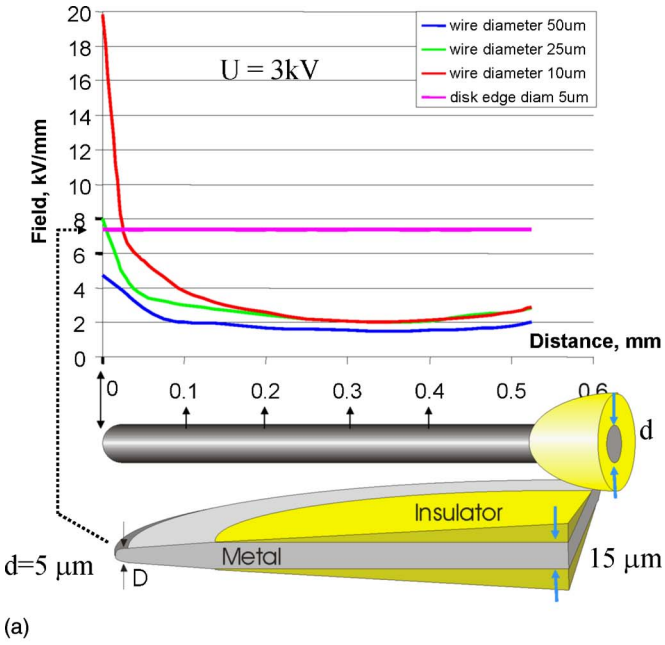


(a)

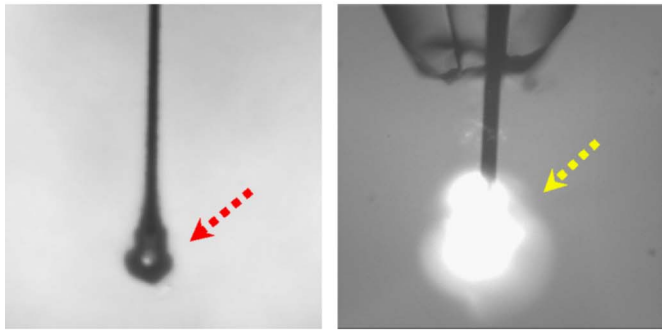

(b)

FIG. 7. (Color online) (a) Electric field on the surface of the wire electrodes of 10, 25, and 50 $\mu$m in diameter and 0.5 mm in length at potential of 100 V. The distance is measured from the apex of the wire electrode. Horizontal line at 7.5 kV/mm represents electric field along the exposed edge of the insulated disk electrode of 5 $\mu$m in thickness. (b) Formation of the vapor bubble (left frame) and plasma (right frame) around the apex of the long wire electrode of 50 $\mu$m in diameter.

energy increases linearly with voltage, $E \sim U$, and plasma ignition delay scales reciprocal to the voltage $t \sim 1/(U - U_{th})$, thus $E$ should decrease with pulse duration.

Interestingly, the threshold energy on a blade electrode had an opposite trend: it increased with pulse duration. The

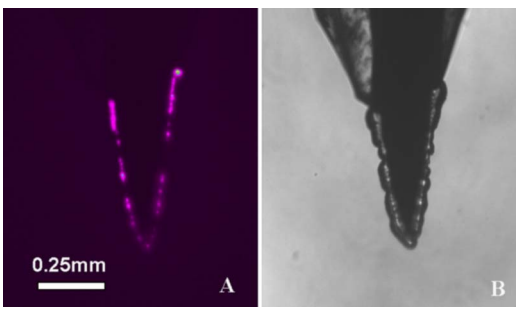


FIG. 8. (Color online) (a) Plasma formation at the perimeter of the blade following a 200 ns pulse of 3.4 kV. (b) Cavitation bubbles forming around the exposed perimeter of the blade, as seen with a fast flash photography 5 $\mu$s after the pulse.

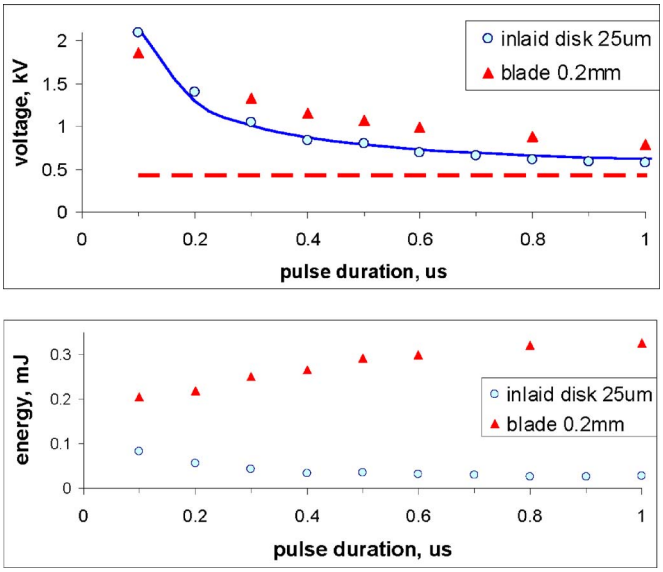


FIG. 9. (Color online) Ionization threshold voltage (a) and energy (b) for a 25 $\mu$m inlaid disk and an insulated blade of 200 $\mu$m in length and having an exposed edge of 5 $\mu$m in thickness. The solid line in (a) depicts a fitting function $U=0.45+0.17/t$; the dashed line at 0.45 kV represents an asymptotic value of the threshold voltage for positive discharge.

reason for this effect is related to the fact that our surgical blade was not a perfect disk, and thus did not have perfectly uniform electric field along its edge. A sharper apex of the blade and some nonuniformities along its boundary had a lower ionization threshold. Since for uniform cutting of tissue ionization along the whole edge is required, we defined ionization threshold on the blade as ionization along the whole boundary, rather than the appearance of the first spark of plasma. Due to the field nonuniformities plasma develops earlier in some parts of the blade, leading to a rapid decrease in impedance in these areas and associated increase in the total discharge energy. Since the threshold energy increased with pulse duration, the application of shorter pulses is advantageous for minimization of collateral damage in surgical applications of the blade electrode.

Such a probe has been successfully tested in cutting soft tissues such as retina, vitreoretinal membranes and chorioallantoic membrane of chicken embryo, achieving complete separation of sides in one scan. The tissue could be dissected along the whole lengths of the blade. Since the depth of the cut in a bulk tissue in this approach is determined by the length of the blade rather than by the size of the cavitation bubble, much deeper cutting could be achieved while maintaining a relatively narrow collateral damage zone. Figure 10 demonstrates a cut in a chorioallantoic membrane achieved with 100 ns pulses at $-4$ kV applied at a repetition rate of 100 Hz. The incision rate was 1 mm/s. Damage zone at the edges, as indicated by the propidium iodide staining, was $70-80$ $\mu$m in width. Such a damage zone can be maintained along any depth of the cut in a bulk tissue, which was impossible with a pointed (inlaid disk) electrode.

## IV. CONCLUSIONS

An elongated blade electrode having micrometer-sharp exposed edges and insulated flat sides provides a much more uniform and enhanced electric field than a wire electrode of equivalent length. Voltages of 3–4 kV suffice for ionization and vaporization of physiological medium using 100 ns pulses. Such a system allows for the dissection of soft biological tissues to arbitrary depth and for continuous cutting leaving no bridges between the two sides. The collateral damage zone at the edges of the cut was limited to $70-80$ $\mu$m. Negative polarity was found advantageous due to significantly lower rate of metal erosion.

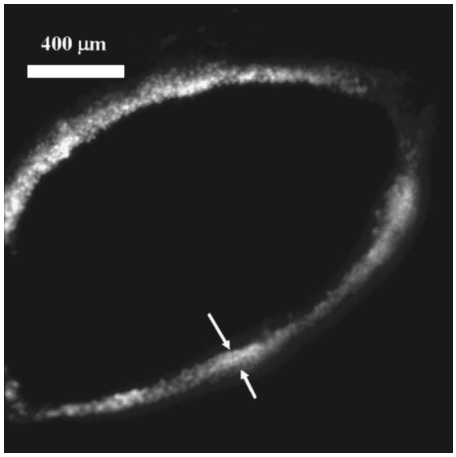


FIG. 10. Cut in CAM produced with a blade electrode of 0.4 mm in length using pulses of $-4$ kV, 100 ns, at a repetition rate of 100 Hz. Pulse energy was 0.3 mJ. Propidium iodide staining reveals collateral damage zone of $70-80$ $\mu$m in width.

## ACKNOWLEDGMENTS

The authors would like to thank Roopa Dalal for histological preparations and photography. Funding was provided by NIH Grant No. 2R01 EY012888–04, Whitaker Foundation Grant No. RG-03–0042, and by the Air Force Office of Scientific Research (MFEL grant).

[1] G. Geerling, J. Roider, U. Schmidt-Erfurt, and K. Nahen, Br. J. Ophthalmol. **82**, 504 (1998).
[2] C. P. Lin, Y. K. Weaver, R. Birngruber, J. G. Fujimoto, and C. A. Puliafito, Lasers Surg. Med. **15**, 44 (1994).
[3] A. Vogel, P. Schweiger, A. Frieser, M. Asiyo, and R. Birngruber, Fortschr. Ophthalmol. **87**, 675 (1990).
[4] C. P. Cain, C. A. Toth, C. D. DiCarlo, G. D. Noojin, R. Amnotte, V. Caruthers, and B. A. Rockwell, Proc. SPIE **2975**, 133 (1997).
[5] P. D. Brazitikos, D. J. D'Amico, M. T. Bernal, and A. W. Walsh, Ophthalmology **102**, 278 (1995).
[6] P. D. Brazitikos, D. J. D'Amico, T. W. Bochow, M. Hmelar, G. R. Marcellino, and N. T. Stangos, Invest. Ophthalmol. Vis. Sci. **39**, 1667 (1998).
[7] I. Hemo, D. Palanker, I. Turovets, A. Lewis, and H. Zauberman, Invest. Ophthalmol. Vis. Sci. **38**, 1825 (1997).
[8] D. J. D'Amico, M. S. Blumenkranz, M. J. Lavin, H. Quiroz-Mercado, I. G. Pallikaris, G. R. Marcellino, and G. E. Brooks, Ophthalmology **103**, 1575 (1996).
[9] D. Palanker, I. Turovets, and A. Lewis, J. Appl. Phys. **81**, 7673 (1997).
[10] D. V. Palanker, J. M. Miller, M. F. Marmor, S. R. Sanislo, P. Huie, and M. S. Blumenkranz, Invest. Ophthalmol. Vis. Sci. **42**, 2673 (2001).
[11] D. V. Palanker, M. F. Marmor, A. Branco, P. Huie, J. M. Miller, S. R. Sanislo, A. Vankov, and M. S. Blumenkranz, Arch. Ophthalmol. **120**, 636 (2002).
[12] J. M. Miller, D. V. Palanker, A. Vankov, M. F. Marmor, and M. S. Blumenkranz, Arch. Ophthalmol. **121**, 871 (2003).
[13] D. J. Arndt-Jovin and T. M. Jovin, Methods Cell Biol. **30**, 417 (1989).
[14] M. J. Waring, J. Mol. Biol. **13**, 269 (1965).
[15] W. Chadband, *From Bubbles to Breakdown, or Vice-Versa* (IEEE, Piscat-

away, NJ, 1993), pp. 184–193.
[16]H. M. Jones and E. E. Kunhardt, J. Appl. Phys. **77**, 795 (1995).
[17]R. E. Tobazeon, in *The Liquid State and its Electrical Properties*, edited by E. E. Kunhart, L. G. Christophoreau, and L. H. Luessen (Plenum, New York, 1987), pp. 465–501.
[18]P. K. Watson, IEEE Trans. Electr. Insul. **20**, 395 (1985).
[19]R. P. Joshi, J. Qian, and K. H. Schoenbach, J. Appl. Phys. **92**, 6245 (2002).
[20]T. J. Lewis, IEEE Trans. Dielectr. Electr. Insul. **5**, 306 (1998).
[21]O. Lesaint, *Propagation of Positive Discharge in Long Liquid Gaps* (IEEE, Piscataway, NJ, 1996), pp. 161–166.
[22]B. R. Scharifker, in *Modern Aspects of Electrochemistry*, edited by J. Bockris (Plenum, New York, 1992), p. 472.
[23]C. E. Brennen, *Cavitation and Bubble Dynamics* (Oxford University Press, New York, 1995).
[24]F. R. Young, *Cavitation* (McGraw-Hill, England, 1989), pp. 13–16.
[25]L. Haar, J. S. Gallagher, and G. S. Kell, *NBS/NRC Steam Tables* (McGraw-Hill, New York, 1984).
[26]J. Janca, S. Kuzmin, A. Maximov, J. Titova, and A. Czernichowski, Plasma Chem. Plasma Process. **19**, 53 (1999).